narra j

Short Communication

In silico analysis of *Arbacia lixula*-derived peptides and plasmid construction for recombinant anti-aging therapies

Satya W. Yenny[1*], Jamsari Jamsari[2], Auliya A. Hazmi[1], Kevin N. Cuandra[3], Wafiq Hanifah[4], Angela S. Yahono[4], Dhyani P. Wahyudi[5], Gherriandi R. Buana[5], Awalil RK. Rahman[6], Annisa D. Maharani[3], Muhammad F. Firjatullah[6], Rafi Maulana[3], Norbertus M. Prayogi[7] and Christopher D. Tristan[6]

[1]Department of Dermatology, Venereology and Esthetic, Faculty of Medicine, Universitas Andalas, Padang, Indonesia; [2]Department of Agrotechnology, Faculty of Agriculture, Universitas Andalas, Padang, Indonesia; [3]Department of Medicine, Faculty of Medicine, Universitas Andalas, Padang, Indonesia; [4]Department of Medicine, Faculty of Medicine, Universitas Gadjah Mada, Yogyakarta, Indonesia; [5]Department of Medicine, Faculty of Medicine, Universitas Pembangunan Nasional Veteran Jakarta, Jakarta, Indonesia; [6]Department of Medicine, Faculty of Medicine, Universitas Sebelas Maret, Surakarta, Indonesia; [7]Department of Medicine, Faculty of Medicine, Universitas Lampung, Lampung, Indonesia

*Corresponding author: satyawidyayenny@med.unand.ac.id

Abstract

Skin aging is one of the degenerative processes influenced by tyrosinase, elastase, collagenase, hyaluronidase, and matrix metalloproteinase-9 (MMP9) activity. One promising avenue for discovering antiaging therapeutics is the peptides from the *Arbacia lixula* spine. The aim of this study was to explore the potential of peptides from *A. lixula* spine as a multitarget inhibitor for recombinant antiaging therapies through in silico approaches. The crystal structure of peptides previously identified in *A. lixula* spine was visualized using the UCSF Chimera. The protein data bank (PDB) database was used to obtain the crystal structures of protein targets. The webservers Innovagen, AllerTop, and ToxinPred were utilized to predict the peptide's water solubility, toxicity, and allergenicity. MOE application was used to prepare all ligands and proteins, molecular docking, and visualization. Molecular dynamics simulations were carried out on the protein-ligand complexes on Yasara Dynamics application. The Benchling website was used to perform virtual electrophoresis and reconstruct the recombinant plasmid (Psb1c3). Based on the molecular docking results, peptide REGSPDLLE has the potential as a multitarget inhibitor of tyrosinase (-9.07 kcal/mol), hyaluronidase (-10.57 kcal/mol), elastase (-9.32 kcal/mol), collagenase (-10.57 kcal/mol), and MMP9 (-10.43 kcal/mol). Peptide REGSPDLLE was selected due to its strong binding affinity on the active site of each target protein and exhibits non-toxic, non-allergenic, and good water-soluble as indicated by Support Vector Machine score <0. Molecular dynamics simulations confirmed stable interactions with receptor proteins. Peptide REGSPDLLE was successfully inserted into the recombinant pSB1C3 plasmid, confirmed by virtual electrophoresis with bands at ~2000 bp and ~150 bp. Further in vitro and in vivo studies are necessary to verify the anti-aging efficacy of peptide REGSPDLLE.

Keywords: Anti-aging, *Arbacia lixula*, molecular docking, peptide-based drug, plasmid

Introduction

Skin aging is believed to occur in the human body starting from the second decade of life, as seen visually by magnifying tools [1]. Both external and internal mechanisms contribute to skin aging.

https://narraj.org/

Received: August 6, 2024 - Accepted: October 24, 2024 - Published online: November 20, 2024

A previous report suggested several proteins and enzymes that play important roles in aging [2]. Some of them are tyrosinase, elastase, collagenase, hyaluronidase, and matrix metalloproteinase-9 (MMP9) [2].

Tyrosinase scavenges reactive oxygen species (ROS) and absorbs up to 75% of UV radiation, providing protection to the skin [3]. Tyrosinase inhibition can effectively treat pigmentation by lowering melanin production and lightening the skin [3]. The connective tissue of skin contains a protein called elastin, which has elastic properties and is crucial for preserving tissue structure after tugging or stretching. The skin's elastin fiber network becomes hydroxylated due to increased elastase expression induced by overexposure to UV light and excessive ROS generation [5]. Strategies for inhibiting elastase have been shown to enhance skin elasticity and the linearity of skin elastic fibers [5]. Inhibiting collagenase also might promote the collagen in the dermis layer, thereby preventing wrinkles in the skin [6]. Another target to prevent skin aging is hyaluronidase, an enzyme responsible for the breakdown of hyaluronic acid in the skin. Hyaluronic acid has been reported to be involved in wound healing and wrinkle reduction by hydration and rejuvenation of skin [7,8]. In addition to the aforementioned targets, MMP9 is also considered as the target to prevent skin aging. MMP9 expression is significantly increased during exposure to UV radiation, which disrupts MMP9 action in human skin tissues [9,10].

Advances in peptide-based drugs have created novel treatment options for skin aging, including those from marine organisms such as sea urchin (*Arbacia lixula*) [11]. Despite being a dangerous animal, sea urchin has been utilized extensively as food and supplements due to their high antioxidant contents, especially polyphenols [12,13]. *Arbacia lixula* is one kind of sea urchin frequently found in tropical waters with a high astaxanthin content [14]. Although the spine of *A. lixula* is known to contain several peptides, little research has been done on the potential of this species to prevent aging. The peptides from *A. lixula* that have been identified as skin aging inhibitors can be produced through recombinant protein. The function of recombinant proteins is to refine and exploit the functional characteristics of the target protein while maintaining (and in some cases improving) safety or efficacy of the treatment, thereby ensuring that the drug's effectiveness therapy is specific and precisely targeted [15]. Therefore, the aim of this study was to explore the potential of peptide-based metabolites from *A. lixula* spine as a multitarget inhibitor agent for antiaging and plasmid construction to enhance specific recombinant peptide production through computational approaches.

Methods

Preparation of ligands and proteins

This study used the sequence peptides from peptidomics profiling of the *A. lixula* spine that has been reported previously [11]. There was a total of 18 peptides labeled sequentially as P1, P2, P3, up to P18. The crystal structure of each *A. lixula* spine peptide was then obtained by visualizing the peptides using the UCSF Chimera tool v1.17.1. The crystal structure of each target protein control ligand was isolated from the protein data bank (PDB) of each protein using the MOE v2022.02 application. All ligands (control ligands and P1-P15) were then prepared by preserving, neutralizing sequence, adding hydrogen, and refining to a Root Mean Square (RMS) gradient of 0.001 kcal/mol/Å2. As for tyrosinase (PDB: 2Y9X), hyaluronidase (PDB: 1FCV), elastase (PDB: 1Y93), collagenase (PDB: 2D1N), and MMP9 (PDB: 1GKC), their crystal structures were retrieved from PDB database. MOE v2022.02 application was used to prepare all proteins by removing all molecule water, preserving and neutralizing sequence, and refining to an RMS gradient of 0.001 kcal/mol/Å2.

Peptide characteristics prediction test

The webservers of Innovagen (http://www.innovagen.com/), AllerTop (https://www.ddg-pharmfac.net/AllerTOP/), and ToxinPred (http://crdd.osdd.net/toxinpred/) were utilized to predict the water solubility, allergenicity, and toxicity characteristics of a peptide. Based on the water solubility prediction test, the peptides were classified as good or poor. Peptides were classified as toxic or non-toxic based on the findings of the toxicity test. Meanwhile, the peptides were classified as allergens or non-allergens based on the findings of the allergenicity test.

Peptides selected as anti-aging therapeutic candidates must fulfill all the characteristic criteria: good water solubility, non-toxic (SVM<0), and non-allergenic (SVM<0). Classifications of the characteristics followed the suggestion of a previous report [16].

Molecular docking

The MOE v2022 application was used to perform molecular docking analysis and 2D & 3D visualization. The binding sites were precisely positioned at each target protein's active site for conducting a specific molecular docking analysis. Using the MOE application's Site Finder feature, the binding site settings were automatically modified based on the amino acid residues in each protein's natural ligand (**Table 1**). Molecular docking outcomes comprised binding affinity (kcal/mol), Root Mean square Deviation (RMSD) (Å), and visualization in two and three dimensions. If a peptide has an RMSD of less than 2.5 Å, it indicates good alignment, supporting the validity of the docking approach. Additionally, if the peptide's binding affinity is more negative compared to the control ligand, it suggests that the peptide has strong binding potential [17]. The 2D visualization results were used to assess the similarity between the interaction bonds formed between the peptide-target protein and the control ligand-target protein. The similarity between the amino acid residues in the active sites of each target protein created by the peptide and the control ligand means that the peptide has the potential to replace the control ligand as a target protein inhibitor. Otherwise, if there was no similarity, 3D visualization was used to confirm whether the peptide could replace the control ligand at the active site of the target protein.

Table 1. The amino acid residues of tyrosinase, hyaluronidase, elastase, collagenase, and matrix metalloproteinase-9 (MMp9) active site

PDB ID	Protein	Amino acid residues
2Y9X	Tyrosinase	HIS61, ASN81, HIS85, GLY86, THR87, PHE90, HIS94, HIS244, GLY245, ALA246, VAL247, VAL248, GLU256, MET257, HIS259, ASN260, HIS263, PHE264, MET280, GLY281, SER282, VAL283, ALA286, PHE292, HIS296, MET319, ASN320, ARG321, GLU322
1FCV	Hyaluronidase	ASP111, GLU113, ARG116, TYR184, ALA185, PRO187, TYR188, CYS189, TYR190, ASN191, THR193, ASN195, PRO224, SER225, VAL226, TYR227, ARG229, LEU240, ARG244, GLN271, ARG274, TRP301, SER303
1Y93	Elastase	GLY179, ILE180, LEU181, ALA182, HIS183, ALA184, LEU214, THR215, HIS218, GLU219, HIS222, HIS228, PRO232, LYS233, ALA234, VAL235, MET236, PHE237, PRO238, THR239, TYR240, LYS241, VAL243, THR247, PHE248, ARG249, LEU250, SER251, ASP254
2D1N	Collagenase	PHE107, SER182, GLY183, LEU184, LEU185, ALA186, HIS187, ALA188, PHE189, PRO190, TYR214, LEU218, VAL219, HIS222, GLU223, HIS226, HIS232, PRO236, GLY237, ALA238, LEU239, MET240, PHE241, PRO242, ILE243, TYR244, THR245, TYR246, THR247, PHE252, PRO255
1GKC	MMP9	PHE110, GLU111, GLY186, LEU187, LEU188, ALA189, HIS190, ALA191, TYR393, LEU397, VAL398, HIS401, GLU402, HIS405, HIS411, PRO415, GLU416, ALA417, LEU418, MET419, TYR420, PRO421, MET422, TYR423, ARG424, THR426, PRO429, PRO430, LEU431, HIS432

PDB ID: protein data bank identifier

Molecular dynamic simulation

Molecular dynamics simulations were performed using YASARA Dynamics v4.3.13. Each sample was initially entered into the application through the Options menu, selecting the Set Target and Macro & Movie options. A macro input was used to run the molecular dynamics simulations, specifying parameters in the variable section, including a physiological pH of 7.4 and a temperature of 310 K. The simulation was set to run for 50,000 ps (50 ns) using the macro md_run. The “MD_analysis” macro was used to calculate the Root Mean Square Deviation (RMSD). The molecular dynamic protocol followed the recommendation of a previous study [18].

Plasmid recombinant design

Gene constructed in *Escherichia coli* K12 followed the Biobrick base format, which includes a prefix, suffix, and the gene of interest [19]. The synthetic biology cloning vector pSB1AC3 was obtained from the Registry of Standard Biological Parts (Massachusetts Institute of Technology, Cambridge); the Chloramphenicol resistance gene already included this vector. The peptide of

interest gene (P15) was obtained by translating the protein into a DNA sequence in https://insilico.ehu.es/ web server. The vector would contain the T7 promoter (BBa_I712074), a ribosome binding site, and the starting methionine triplet (ATG) and terminating triplet (TAA). These sequences were converted into txt files before being exported to the Benchling website (https://benchling.com/) to reconstruct recombinant plasmids.

We included the T7 RNA polymerase promoter for the regulatory region, which is believed to be one of the strongest available [20]. We extended the upstream region of the core promoter with a sequence overlapping the NheI restriction site. A T-A-rich stretch in this region increases promoter strength while incorporating several G-C residues weakens the promoter. In this study, the core promoter was extended by the sequence CTAGC, containing both AT and GC, which is expected not substantially to decrease the promoter strength.

Results

Toxicity, allergenicity, and water solubility prediction test

All *A. lixula* spine peptides were predicted to be non-toxic based on the toxicity prediction test (**Table 2**). As a result of the *A. lixula* peptide test, it was found that 12 out of 18 peptides were predicted non-allergenic (P1, P4, P5, P6, P9, P12, P13, P14, P15, P16, P17, and P18). However, the remaining six peptides were predicted to be allergenic, which excluded them from the list of potential peptides. Eight peptides (P3, P7, P8, P9, P11, P13, P14, and P15) showed good water solubility. On the other hand, the remaining 10 peptides were insoluble in water, ruling them out from the list of potential peptides (**Table 2**).

Table 2. Toxicity, allergenicity, and water solubility prediction tests of peptides from *A. lixula* spine

Ligand	Peptide sequence	Toxicity	Allergenicity	Water solubility
P1	GLAH	Non-toxic	Non-allergenic	Poor
P2	NLVM	Non-toxic	Allergenic	Poor
P3	NRDT	Non-toxic	Allergenic	Good
P4	TAAH	Non-toxic	Non-allergenic	Poor
P5	FLMEV	Non-toxic	Non-allergenic	Poor
P6	LLGHH	Non-toxic	Non-allergenic	Poor
P7	TSLEP	Non-toxic	Allergenic	Good
P8	DTGSAD	Non-toxic	Allergenic	Good
P9	ECNGPGW	Non-toxic	Non-allergenic	Good
P10	ELMVVC	Non-toxic	Allergenic	Poor
P11	MAAPSD	Non-toxic	Allergenic	Good
P12	MTSKPTW	Non-toxic	Non-allergenic	Poor
P13	REGSPDLR	Non-toxic	Non-allergenic	Good
P14	GLKGSPDLR	Non-toxic	Non-allergenic	Good
P15	REGSPDLLE	Non-toxic	Non-allergenic	Good
P16	TNLLGTGAH	Non-toxic	Non-allergenic	Poor
P17	MQLFVGSNLE	Non-toxic	Non-allergenic	Poor
P18	PYLFGGMLQL	Non-toxic	Non-allergenic	Poor

Molecular docking result

Molecular docking result of tyrosinase

The molecular docking results of the binding affinity of all peptides from *A. lixula* spine with the protein targets are presented in **Table 3**. All peptides exhibited RMSD values lower than 2.5 Å. The binding affinity of all the peptides was stronger compared to kojic acid (-5.31 kcal/mol) at the tyrosinase active site. P15 was found to have a higher binding affinity on the active site of tyrosinase (-9.07 kcal/mol) as compared to kojic acid (-5.31 kcal/mol). Therefore, in addition to its non-toxic, non-allergenic, and good water solubility properties, P15 was selected for the representation. Based on 2D visualization analysis, P15-tyrosinase created eight interactions: one acidic hydrophilic interaction (Glu322), one basic hydrophilic interaction (Arg268), five polar hydrophilic interactions (His85, Asn200, Gly249, Thr264, Ser282), and one hydrophobic interaction (Ala252). Meanwhile, amino acids involved in the kojic acid-tyrosinase complex were one acidic hydrophilic (Glu402), two polar hydrophilic (Gly186, Tyr423), and three hydrophobic

interactions (Leu188, Pro421, Met422). Based on the similarity of the interaction, there are no similarities between amino acid residues involved in P15-tyrosinase and kojic acid-tyrosinase (**Figure 1**). However, the 3D analysis showed that P15 fitted perfectly within the tyrosinase's active site, reinforcing its potential as a specific inhibitor (**Figure 1**).

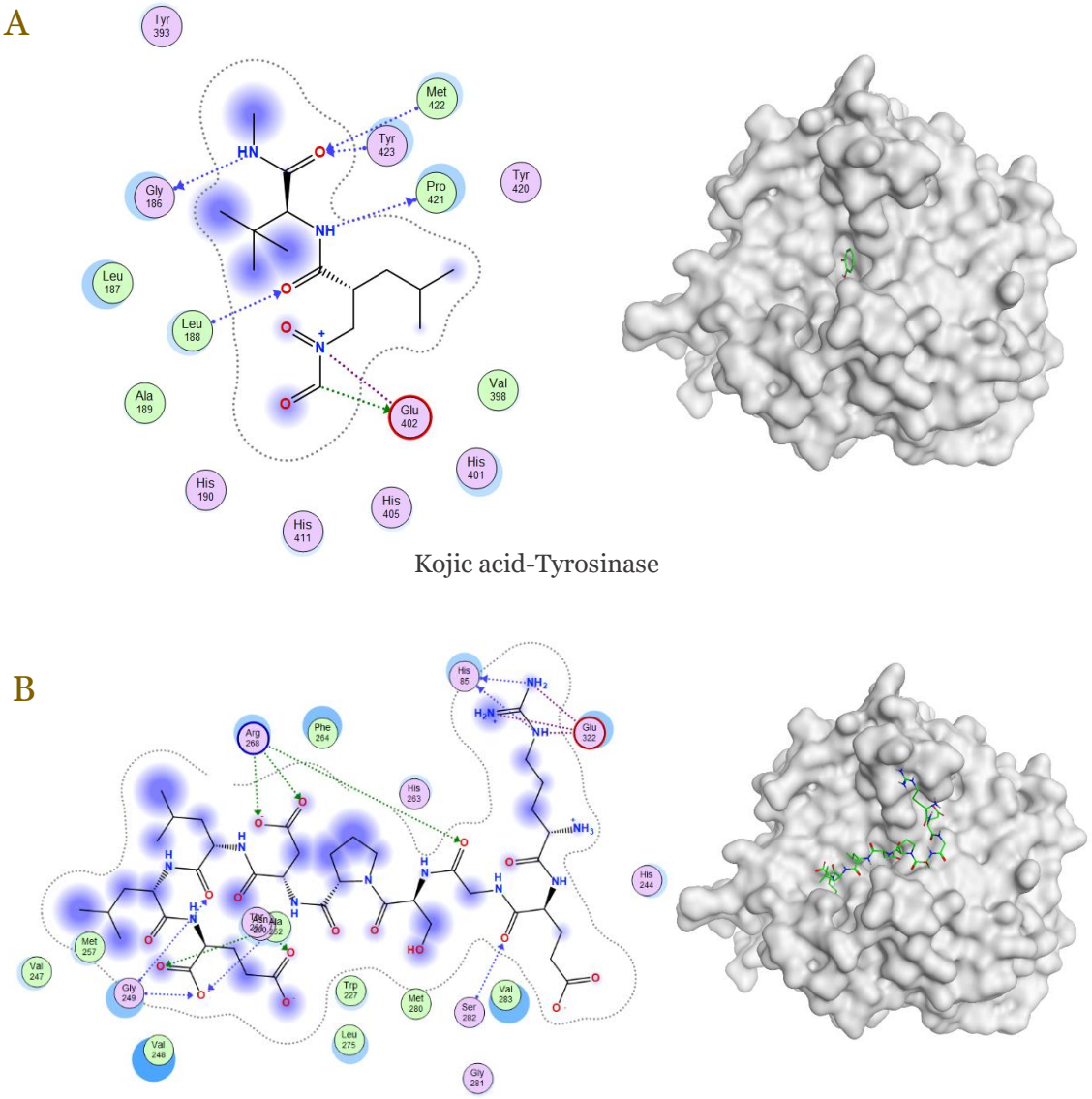

Figure 1. 2D and 3D visualization results: tyrosinase complex with kojic acid (A) and P15 (B).

Molecular docking result of hyaluronidase

Molecular docking between the *A.lixula* spine peptides and hyaluronidase showed that all peptides had stronger binding affinities than kojic acid at the active site. However, the findings indicated that the RMSD values for P9, P13, and P17 were greater than 2.5 Å (**Table 3**). Compared to all the *A. lixula* spine peptides, P15 had the highest binding affinity (-10.57 kcal/mol) and had RMSD lower than 2.5 Å (2.28 Å). P15 also had good water solubility and non-allergen and non-toxic characteristics.

According to the 2D interaction visualization (**Figure 2**), P15 created nine interactions with the hyaluronidase active site: two acidic hydrophilic interactions (Asp111, Glu113), two basic hydrophilic interactions (Arg274, Arg244), four polar hydrophilic interactions (Asn195, Ser303, Ser225, Gln271), and one basic hydrophobic interaction (Trp301). Kojic acid, on the other hand, interacted with the hyaluronidase active site through three interactions: two polar hydrophilic interactions (Ser 225 and Tyr 188) and one basic hydrophilic interaction (Arg244).

Table 3. The binding affinity and RMSD value from molecular docking results of tyrosinase, hyaluronidase, collagenase, elastase, and matrix metalloproteinase-9 (MMP9)

Ligand	Tyrosinase		Hyaluronidase		Collagenase		Elastase		MMP9	
	BA	RMSD	BA	RMSD	BA	RMSD	BA	RMSD	BA	RMSD
Control	-5.31	1.33	-4.84	1.74	-9.07	1.86	-3.74	0.70	-6.69	1.56
P1	-7.16	1.34	-7.28	1.72	-8.12	1.36	-7.36	1.61	-8.11	2.24
P2	-7.30	1.49	-7.96	1.79	-8.32	1.63	-7.20	1.85	-8.41	1.52
P3	-7.88	1.86	-7.91	1.92	-8.11	1.87	-7.90	1.60	-8.28	1.89
P4	-7.07	1.87	-7.26	1.62	-7.05	1.20	-7.16	1.84	-7.44	1.92
P5	-8.35	2.10	-8.67	1.99	-8.95	2.74	-7.64	1.81	-8.58	1.84
P6	-7.75	1.65	-8.75	2.36	-8.90	1.77	-8.57	1.59	-8.51	1.85
P7	-7.23	1.83	-8.18	1.79	-8.19	1.85	-6.90	1.37	-8.45	1.75
P8	-7.59	1.52	-7.89	1.79	-9.68	1.98	-8.81	1.51	-7.87	1.79
P9	-7.76	2.00	-8.79	3.04	-9.72	2.16	-9.13	2.20	-8.59	2.91
P10	-8.37	1.27	-8.05	1.84	-9.06	2.00	-8.24	1.99	-8.06	1.96
P11	-7.75	1.62	-8.09	2.06	-8.56	1.55	-8.57	1.79	-9.23	2.25
P12	-7.99	1.75	-9.07	1.74	-8.70	1.94	-9.23	1.94	-10.21	3.05
P13	-9.23	2.34	-9.78	2.55	-10.36	2.00	-9.65	3.40	-8.78	1.55
P14	-9.12	2.34	-9.81	1.63	-9.72	3.81	-8.75	3.59	-11.04	2.44
P15	-9.07	1.60	-10.57	2.28	-10.57	1.83	-9.32	2.48	-10.43	2.22
P16	-8.86	2.09	-9.22	1.84	-11.47	3.09	-8.63	1.59	-8.96	1.86
P17	-9.82	2.10	-10.46	2.82	-9.67	3.48	-10.12	2.51	-9.14	1.93
P18	-10.70	2.17	-9.95	1.90	-9.82	2.89	-11.23	2.49	-9.58	2.97

BA: binding affinity (kcal/mol); RMS: root mean standard deviation (Å)

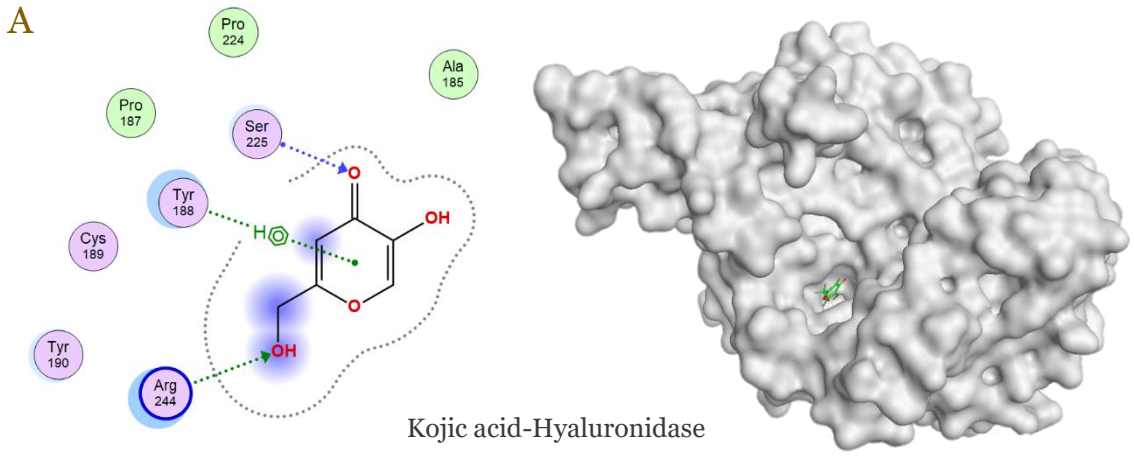

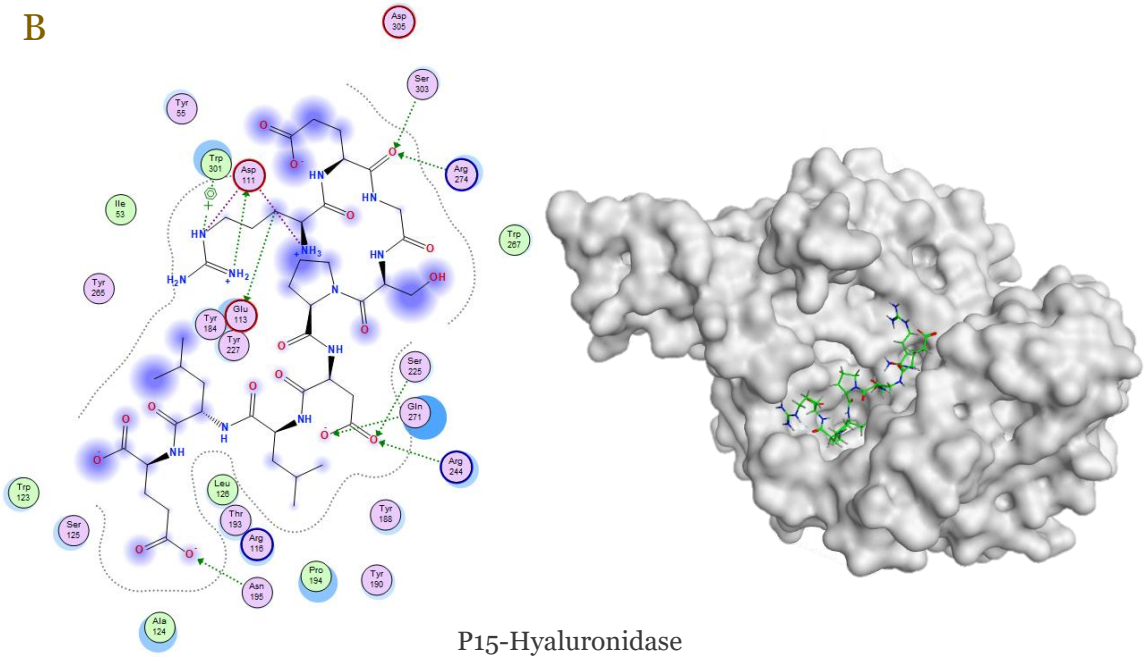

Figure 2. The 2D and 3D visualization results: hyaluronidase complex with (A) kojic acid and (B) P15.

P15 also created the same amino acid residue as kojic acid at the hyaluronidase active site in Ser 225 and Arg 244 (**Figure 2**). These findings suggested that P15 can replace the control ligand in the active site of hyaluronidase and has the potential as a specific hyaluronidase inhibitor.

Molecular docking result of collagenase

Molecular docking between the *A.lixula* spine peptides and collagenase showed that peptides P1, P2, P3, P4, P6, P7, P8, P9, P10, P11, P12, P13, and P15 had RMSD values <2.5 Å (**Table 3**). P15 was selected because it bonded to the active site of the collagenase with a higher binding affinity (-10.57 kcal/mol) than hydroxamic acid (-9.07 kcal/mol) (**Table 3**). According to the 2D interaction visualization, P15 created five interactions with the collagenase active site: one acidic hydrophilic interaction (Asp179), one polar hydrophilic interaction (Tyr244), and one hydrophobic interaction (Pro108, Pro181, and Leu185). Hydroxamic acid created one acidic hydrophilic interaction (Glu223), one polar hydrophilic interaction (Thr245), and three basic hydrophobic interactions (Ala186). According to the similarities of the interactions, there were no similar interactions between P15 and hydroxamic acid in collagenase's active site. Although they did not have similar amino acid residues, P15 fitted perfectly within the collagenase's active site, reinforcing its potential as a specific inhibitor (**Figure 3**).

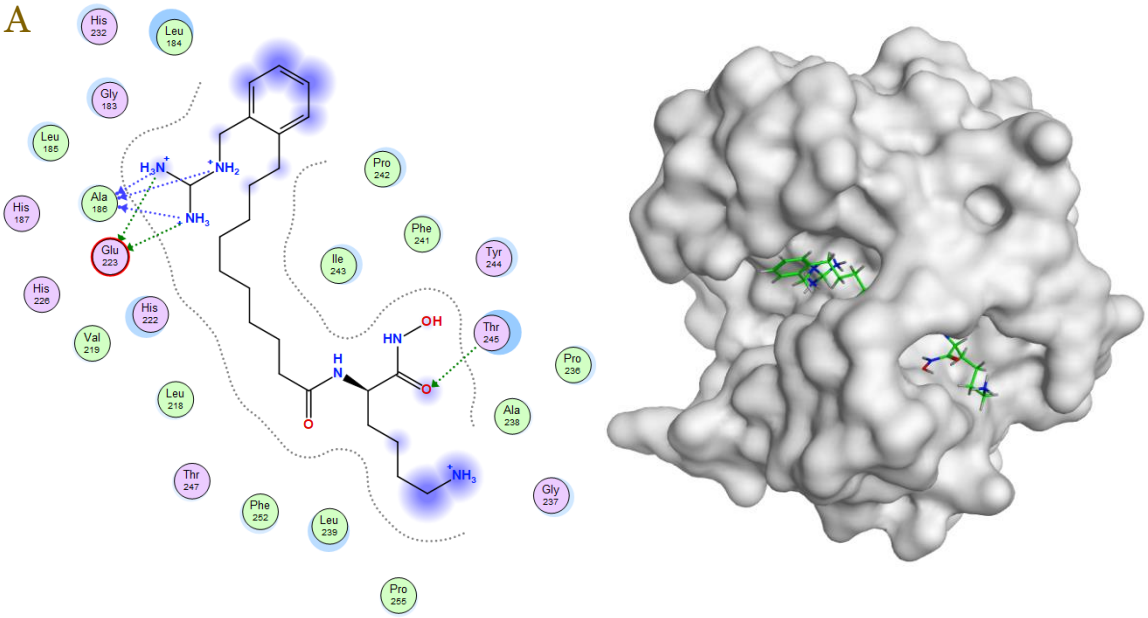

Figure 3. The 2D and 3D visualization results: collagenase complex with (A) hydroxamic acid and (B) P15.

Molecular docking result of elastase

The docking results between the *A. lixula* spine peptides and elastase showed that all peptides had higher binding affinities than acetohydroxamic acid (control ligand) at the elastase active site. These findings showed that the RMSD values for P13, P14, and P17 were more than 2.5 Å. Compared to all the *A. lixula* spine peptides, P15 had good water solubility, non-allergen, and non-toxic properties with an RMSD score <2.5 Å (**Table 1** and **Table 2**).

Based on the 2D interaction visualization, P15 created three interactions with the elastase active site: two basic hydrophilic interactions (His222 and His228) and one polar hydrophilic interaction (Gly179). Acetohydroxamic acid, on the other hand, interacted with the elastase active site through one hydrophobic interaction in Phe237. Although there is no similarity in the amino acid residues involved, based on 3D visualization analysis, P15 was able to potentially replace the role of acetohydroxamic acid as a specific inhibitor of elastase enzyme (**Figure 4**).

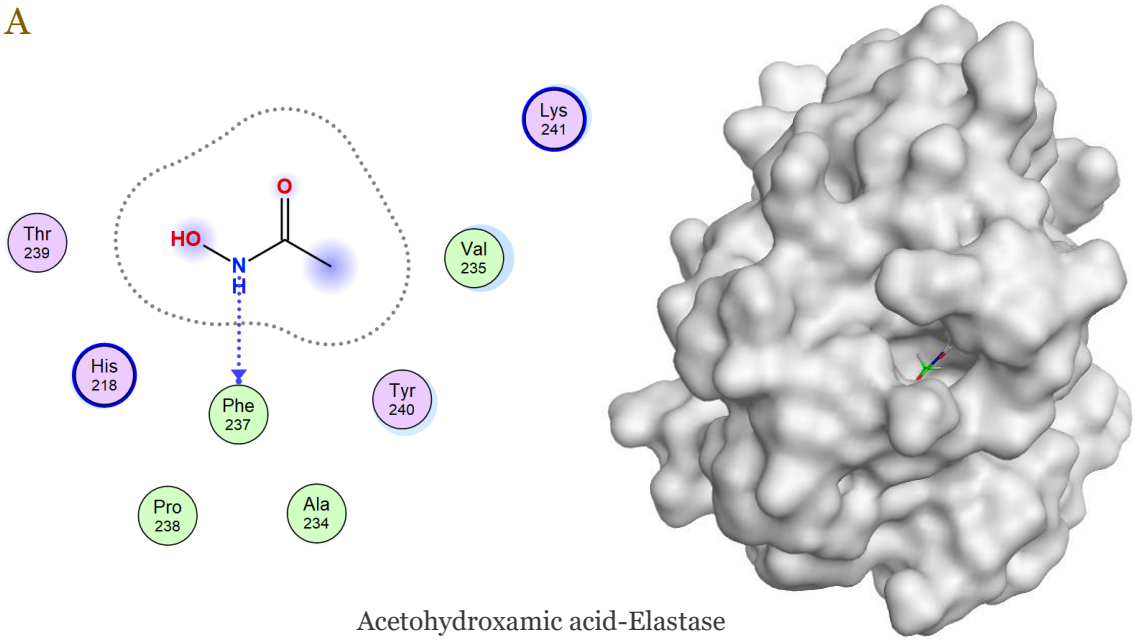

Figure 4. The 2D and 3D visualization results: elastase complex with (A) acetohydroxamic acid and (B) P15.

Molecular docking result of MMP9

The molecular docking results indicated that all peptides had a higher binding affinity score than the N-formyl-N-hydroxy-(2R)-2-isobutyl-beta-alanyl-2-tert-butyl-L-glycine methylamide (-6.69 kcal/mol). Among these, P15 was selected based on the strong binding affinity (-10.43 kcal/mol), RMSD <2.5 Å (2.22 Å), good water solubility, non-allergen, and non-toxic properties (**Table 2** and **Table 3**). P15 created seven interactions with the MMP9 active site: two acidic hydrophilic interactions (Glu111, Glu402) and five hydrophobic interactions (Phe110, Leu187, Leu188, Ala191, and Pro421).

In comparison, N-formyl-N-hydroxy-(2R)-2-isobutyl-beta-alanyl-2-tert-butyl-L-glycine methylamide (control ligand) interacted with the MMP9 active site through one acidic hydrophilic interaction (Glu402), two polar hydrophilic interactions (Gly186, Tyr423), and three hydrophobic interactions (Leu188, Pro421, Met422). P15 interacted with MMP9 similarly to the control ligand at Glu402, Leu188, and Pro421. This data was supported by 3D visualization analysis that proved P15 could replace the role of acetohydroxamic acid as a specific inhibitor of MMP9 protein (**Figure 5**).

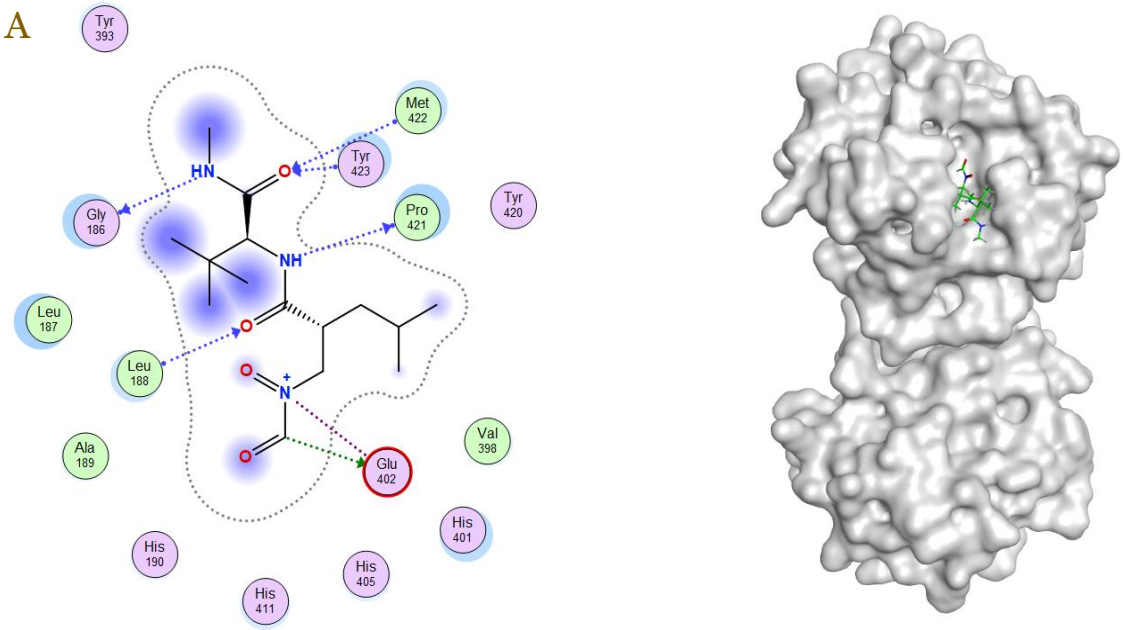

Figure 5. The 2D and 3D visualization results: MMP9 complex with (A) N-formyl-N-hydroxy-(2R)-2-isobutyl-beta-alanyl-2-tert-butyl-L-glycine methylamide and (B) P15.

Molecular dynamics

Results of a molecular dynamics simulation, focusing on the root mean square deviation (RMSD) from the initial complex structure, are presented in **Figure 6**. Throughout the simulation, all RMSD values remain below 6 Å. The C-alpha RMSD (green) shows slightly higher variability compared to the backbone (red) and all heavy atoms (blue), which could suggest some flexibility in specific regions of the protein.

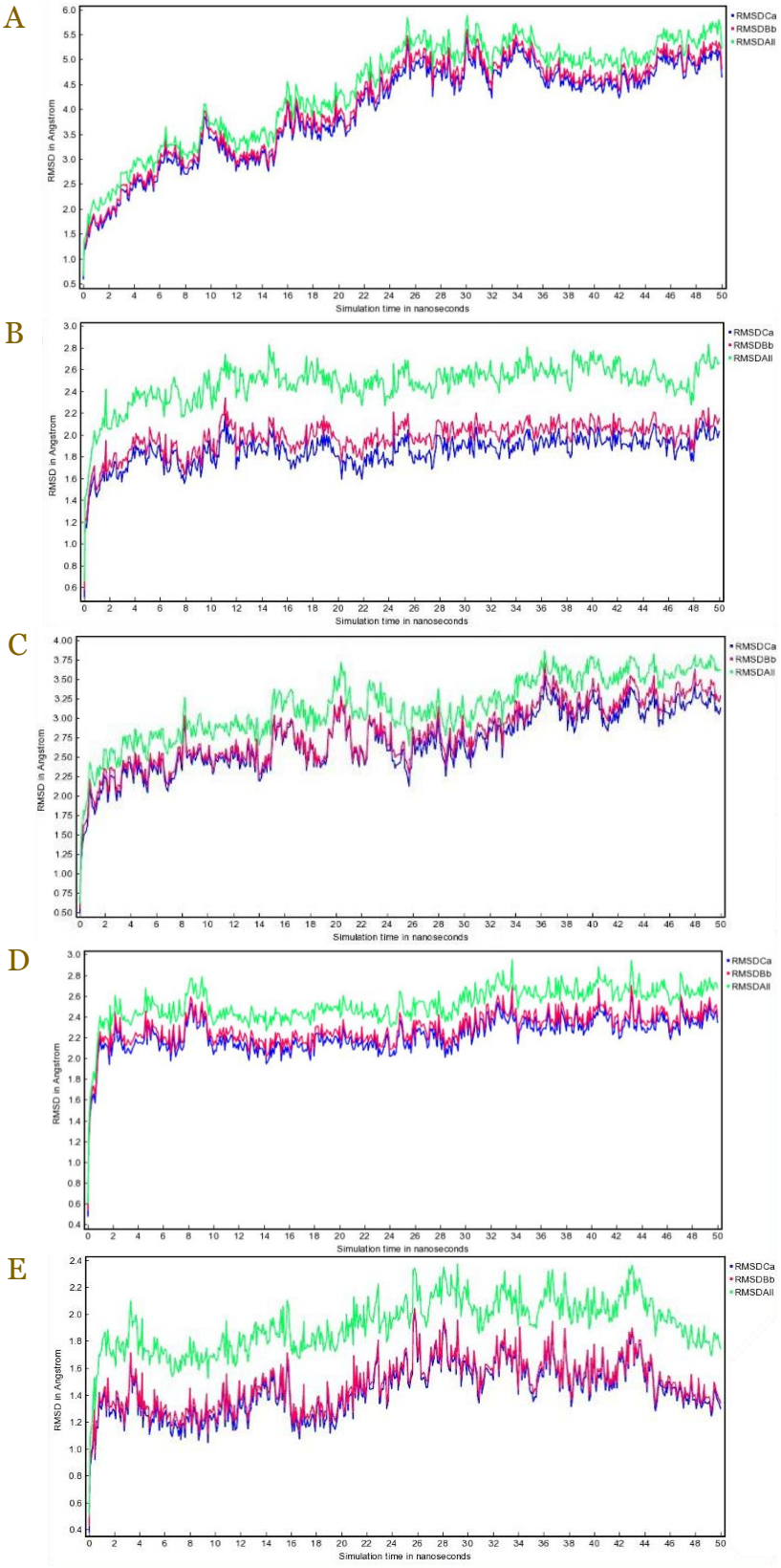

Figure 6. The molecular dynamics simulation of the P15 with (A) matrix metalloproteinase-9 (MMP9), (B) collagenase, (C) elastase, (D) tyrosinase, and (E) hyaluronidase.

Plasmid construction

The results of plasmid construction that has inserted the gene encoding P15 are presented in **Figure 7**. Based on the plasmid construction from the Benchling webserver, a recombinant pSB1C3 plasmid (~2164 bp) design was obtained, with several restriction sites (EcoRI and PstI enzymes). The success rate of the recombinant pSB1C3 plasmid construction was determined from the qualitative results of virtual amplification, showing bands of ~2000 bp and ~150 bp for the peptide-coding gene.

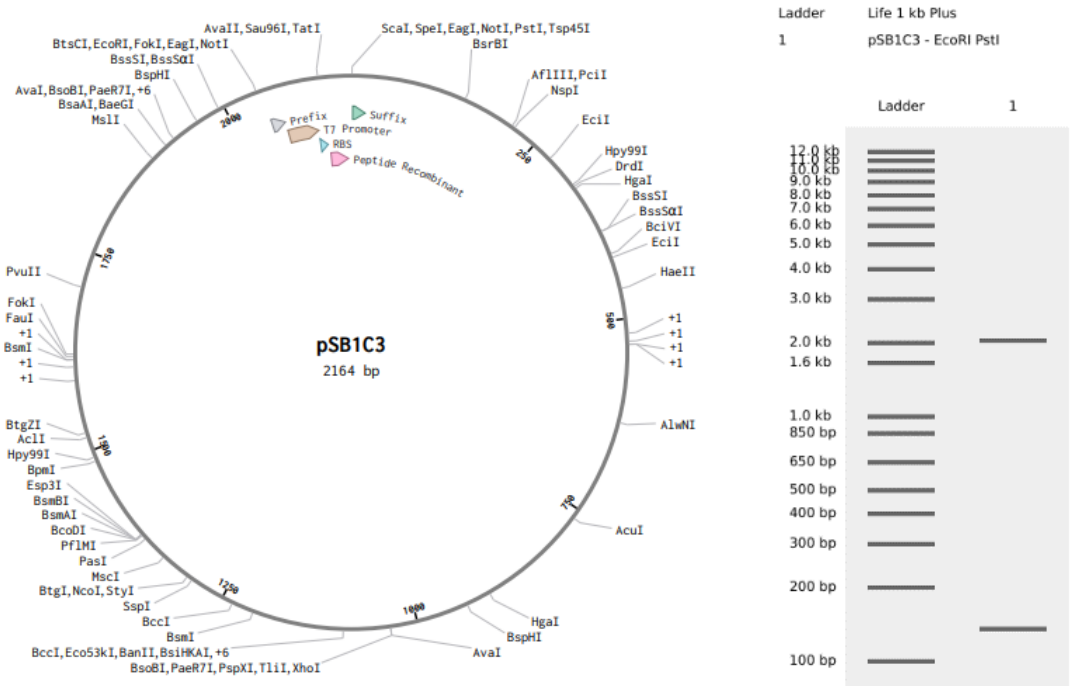

Figure 7. Plasmid design and virtual electrophoresis.

Discussion

Among the peptides examined in the present study, P15 is the most promising specific tyrosinase, hyaluronidase, elastase, collagenase, and MMP9 inhibitor candidate that demonstrates non-toxic, non-allergenic, and good water solubility properties. This finding is evident from the binding affinity value of P15, which is stronger compared to the control ligand. Additionally, P15 also binds more effectively than the control ligand to the specific amino acid residues of each enzyme: tyrosinase (Glu322, Arg 268, His85, Asn200, Gly249, Thr264, Ser282, Ala252), hyaluronidase (Asp111, Glu113, Arg274, Arg244, Asn195, Ser303, Ser225, Gln271, Trp301), elastase (His222, His228, and Gly179), collagenase (Asp179, Tyr244, Pro108, Pro181, Leu185), and MMP9 (Glu111, Glu402, Phe110, Leu187, Leu188, Ala191, and Pro421). These two findings proved that P15 can bind more strongly to tyrosinase, hyaluronidase, elastase, collagenase, and MMP9 active sites compared to the control ligand. Its potential as a tyrosinase inhibitor suggested that P15 may reduce melanin production. The mechanism of tyrosinase inhibition resulting in the alleviation of skin aging via the reduction of melanin production has been previously outlined [3]. Since hyaluronidase is the main regulator of hyaluronic acid turnover in human skin, hyaluronidase inhibitors could delay the breakdown of hyaluronic acid and promote skin moisture retention [7,8]. A previous study reported that elastase inhibitors can be used as cosmetic ingredients to prevent skin aging as they are used to prevent loss of elasticity and sagging of the skin [2,5]. A previous study also stated that the use of collagenase inhibitors can help maintain skin elasticity and prevent signs of aging [6]. Prior in vivo research has demonstrated that MMP9 inhibitors demote the progressive collagen fragmentation in the dermis, further decelerating skin aging [9,10].

The data herein is adequate to depict the stability of P15 in the context of the simulation. Consequently, it can also be taken into consideration while analyzing the possibility of P15 as an inhibitor of tyrosinase, hyaluronidase, elastase, collagenase, and MMP9. The total RMSD value

of the treatment conditions in the P15 anchorage remains below 6 Å, suggesting a substantial conformational shift as well as bond relaxation. An RMSD value gives details on conformational changes that occur in a macromolecule that becomes a receptor after engaging with a certain ligand [18].

Findings from the present study suggested that P15 can be produced explicitly through the recombinant protein process. The codon optimization employed in this work was predicated on the expression systems of the Escherichia coli strain K12, a dominant choice for recombinant protein production due to its fast growth, simplicity in reaching high cell density, and availability of rich media components. Our plasmid construction yielded two distinct fragment bands of ~2000 bp and ~150 bp (totaling in ~2150 bp), confirming the successful expression of the gene encoding P15 from *A. lixula* spine. This approach aligns with current trends in optimizing protein expression in *E. coli*, as highlighted by the previous study, which demonstrated significant yield increases through codon optimization [21]. Previous study also supported the choice of E. coli, noting advantages such as shorter production cycles and minimal risk of viral contamination [22]. However, challenges like inclusion body formation should be considered in future work [23]. The successful construction of the P15-expressing plasmid represented a significant step towards developing novel marine-derived bioactive compounds, particularly for skincare and anti-aging applications.

One limitation of this study is its reliance on an in silico approach, which restricts the interpretation of the results. The absence of in vitro or in vivo validation raises concerns about the accuracy and reliability of the predictions. Validation is crucial, as it requires comparing model outputs with experimental data to determine accuracy. Furthermore, the identification of *A. lixula*-derived peptides was based on a single reference without direct sampling. This may have introduced bias, potentially overlooking other relevant peptides. Comprehensive sampling and peptide sequencing, along with in vitro or in vivo investigation, are required in future studies.

Conclusion

In conclusion, P15 (REGSPDLLE) is predicted to cause no adverse effects, intoxication, or allergic reactions. It also demonstrated good water solubility, a key factor for effective peptide absorption, distribution, and activity in biological systems. Among the control ligands and peptides tested, P15 consistently showed the most favorable outcomes, highlighted by its strong binding affinity and potential as a multitarget inhibitor of tyrosinase, hyaluronidase, elastase, collagenase, and MMP9. Molecular dynamics simulations also supported the structural stability of P15 when interacting with these receptors. Additionally, P15 has the potential for recombinant production via E. coli K12 plasmid construction. Nevertheless, further in vitro and in vivo studies are warranted to confirm its anti-aging effectiveness and efficacy.

Ethics approval

Not required.

Acknowledgments

The authors appreciate dr. Prestasi for their support of this manuscript.

Competing interests

All the authors declare that there are no conflicts of interest.

Funding

This study received no external funding.

Underlying data

Derived data supporting the findings of this study are available from the corresponding author on request.

How to cite

Yenny SW, Jamsari J, Hazmi AA, *et al*. In silico analysis of *Arbacia lixula*-derived peptides and plasmid construction for recombinant anti-aging therapies. Narra J 2024; 4 (3): e1283 - http://doi.org/10.52225/narra.v4i3.1283.

References

1. Yenny SW, Julia DS, Lestari AF, et al. A clinical and novel dermoscopic investigation of combined peels as a hand aging treatment. J Cosmet Dermatol 2024;23(11):3598-3607.
2. Pintus F, Floris S, Fais A, *et al*. Hydroxy-3-Phenylcoumarins as multitarget compounds for skin aging diseases: Synthesis, molecular docking and tyrosinase, elastase, collagenase and hyaluronidase inhibition, and sun protection factor. Molecules 2022;27(20):6914.
3. Rosa GP, Palmeira A, Resende DISP, *et al*. Xanthones for melanogenesis inhibition: Molecular docking and QSAR studies to understand their anti-tyrosinase activity. Bioorg Med Chem 2021;29:115873.
4. Wei M, He X, Liu N, Deng H. Role of reactive oxygen species in ultraviolet-induced photodamage of the skin. Cell Div 2024;19(1):1.
5. Imokawa G, Ishida K. Biological mechanisms underlying the ultraviolet radiation-induced formation of skin wrinkling and sagging i: Reduced skin elasticity, highly associated with enhanced dermal elastase activity, triggers wrinkling and sagging. Int J Mol Sci 2015;16:7753–7775
6. Andrade JM, Domínguez-Martín EM, Nicolai M, *et al*. Screening the dermatological potential of Plectranthus species components: Antioxidant and inhibitory capacities over elastase, collagenase and tyrosinase. J Enzyme Inhib Med Chem 2021;36:257–270.
7. Galvez-Martin P, Soto-Fernandez C, Romero-Rueda J, *et al*. A novel hyaluronic acid matrix ingredient with regenerative, anti-aging and antioxidant capacity. Int J Mol Sci 2023;24(5):4774.
8. Son MH, Park SW, Jung YK. Antioxidant and anti-aging carbon quantum dots using tannic acid. Nanotechnology 2021;32:415102.
9. Chaiyana W, Chansakaow S, Intasai N, *et al*. Chemical constituents, antioxidant, anti-MMPs, and anti-hyaluronidase activities of thunbergia laurifolia Lindl. Leaf extracts for skin aging and skin damage prevention. Molecules 2020;25(8):1923
10. Cancemi P, Aiello A, Accardi G, *et al*. The role of matrix metalloproteinases (MMP-2 and MMP-9) in ageing and longevity: Focus on sicilian long-living individuals (LLIs). Mediators Inflamm 2020;2020:8635158.
11. Sciani JM, Emerenciano AK, Cunha da Silva JR, Pimenta DC. Initial peptidomic profiling of Brazilian sea urchins: *Arbacia lixula*, *Lytechinus variegatus* and *Echinometra lucunter*. J Venom Anim Toxins Incl Trop Dis 2016;22:17.
12. Yenny SW, Suryani YE. Polyphenols as Natural Antioxidants in Skin Aging. Sumat Med J 2020;3(3):4047.
13. Quarta S, Scoditti E, Zonno V, *et al*. In vitro anti-inflammatory and vasculoprotective effects of red cell extract from the Black Sea Urchin *Arbacia lixula*. Nutrients 2023;15:1672.
14. Cirino P, Brunet C, Ciaravolo M, *et al*. The Sea Urchin *Arbacia lixula*: A novel natural source of astaxanthin. Mar Drugs 2017;15:187.
15. Lagassé HAD, Alexaki A, Simhadri VL, *et al*. Recent advances in (therapeutic protein) drug development. F1000Res 2017;6:113.
16. Langyan S, Khan FN, Yadava P, *et al*. In silico proteolysis and analysis of bioactive peptides from sequences of fatty acid desaturase 3 (FAD3) of flaxseed protein. Saudi J Biol Sci 2021;28:5480-5489.
17. Kryshtafovych A, Fidelis K. Protein structure prediction and model quality assessment. Drug Discov Today 2009;14:386-393.
18. Darmadi D, Lindarto D, Siregar J, *et al*. Study of the molecular dynamics stability in the inhibitory interaction of tenofovir disoproxil fumarate against CTLA-4 in chronic hepatitis B patients. Med Arch 2023;77(3):227-230.
19. Shetty RP, Endy D, Knight TF. Engineering BioBrick vectors from BioBrick parts. J Biol Eng 2008;2:5.
20. McManus JB, Emanuel PA, Murray RM, Lux MW. A method for cost-effective and rapid characterization of engineered T7-based transcription factors by cell-free protein synthesis reveals insights into the regulation of T7 RNA polymerase-driven expression. Arch Biochem Biophys 2019;674:108045.
21. Liu B, Kong Q, Zhang D, Yan L. Codon optimization significantly enhanced the expression of human 37-kDa iLRP in Escherichia coli. 3 Biotech 2018;8(4):210.
22. Bhatwa A, Wang W, Hassan YI, *et al*. Challenges associated with the formation of recombinant protein inclusion bodies in escherichia coli and strategies to address them for industrial applications. Front Bioeng Biotechnol 2021;9:630551.
23. Zhang ZX, Nong FT, Wang YZ, *et al*. Strategies for efficient production of recombinant proteins in Escherichia coli: Alleviating the host burden and enhancing protein activity. Microb Cell Fact 2022;21:191.